Resonant inelastic x-ray scattering spectra of magnesium diboride

K. Kokko,* V. Kulmala, and J. A. Leiro
Department of Physics, University of Turku, FIN-20014 Turku, Finland

W. Hergert
Department of Physics, Martin-Luther-University, Friedemann-Bach-Platz 6, D-06099 Halle, Germany

(Received 1 May 2003; published 8 August 2003)

Using the tight-binding linear muffin-tin orbital method, the soft x-ray fluorescence *K*-emission spectra of boron in MgB_2, excited close to the absorption edge, are estimated. In the calculations, the angle of incidence θ between the direction of the incoming photon and the hexagonal axis of the specimen is 60° and 75°. Comparison with experiment is possible in the former case, where good agreement is found. The physically different sheets of the Fermi surface are shown to induce well separated peaks in the resonant inelastic x-ray scattering spectrum. Furthermore, a resonant feature below the Fermi energy is predicted for the larger angle. This feature can be related to the excitations to the antibonding B π-band in the neighborhood of the *L*-*H* line in the Brillouin zone.

DOI: 10.1103/PhysRevB.68.052503 PACS number(s): 74.25.Jb, 71.20.Gj, 78.70.Ck, 78.70.En

Magnesium diboride is a new kind of superconductor, having a critical temperature of 39 K.[1] Although it was earlier widely used in chemical technology, the superconducting property of this compound was not discovered until now.[2] At the moment, MgB_2 has attracted considerable attention regarding spectroscopic investigations.[3] For instance, angle-resolved photoemission from single crystals have revealed clear dispersions of the occupied valence bands.[4] Additional information has been obtained using x-ray absorption spectroscopy (XAS) and x-ray emission spectroscopy (XES).[5] In x-ray *K*-absorption, a core hole is created for the 1*s* level by a photon and the resulting photoelectron is escaping from the specimen. The *K*-emission band can be measured when the deep lying level will be filled by a valence electron and another photon is emitted. The resonant inelastic x-ray scattering (RIXS) differs from the conventional XES in the sense that the photoelectron remains in the conduction band above the Fermi surface and will be absorbed by the sample.[6]

Utilizing synchrotron radiation, resonant inelastic x-ray scattering is a promising method to probe element-specific, local momentum-resolved electronic structure of systems that are difficult to investigate using other techniques. The symmetry of the occupied and unoccupied states is coupled with the polarization and direction of the incoming and outgoing radiation. Crystal momentum conservation has been observed in many materials, e.g., in hexagonal boron nitride and graphite.[7] Theoretical consideration of the RIXS within the band-structure picture is given, e.g., in Ref. 8.

In RIXS, a photon ($\hbar\omega_q$) comes to the sample, excites a core-level (ϵ_a) electron to the conduction state (ϵ_c), and a valence electron (ϵ_v) drops to the core hole, emitting a photon ($\hbar\omega_{q'}$). The formula for the doubly differential cross section in the dipole approximation [the wave vectors of the incoming and outgoing photons are small, $q \approx q' \approx 0$, compared to the dimensions of the Brillouin zone of the Bloch states ($\vec{k}$) of the electrons] implemented in our x-ray spectrum program[9] is

$$\frac{d^2\sigma}{d\Omega d(\hbar\omega_{q'})} \propto \frac{\omega_{q'}}{\omega_q} \sum_{b_c,b_v,\vec{k},m_s} \left| \sum_{t,m_j} M^{b_v,\vec{k}}_{t,m_j,m_s} M^{*b_c,\vec{k}}_{t,m_j,m_s} \right|^2 \times \delta(\epsilon_a - \epsilon_c + \hbar\omega_q)\,\delta(\epsilon_a - \epsilon_v + \hbar\omega_{q'}), \quad (1)$$

where b_c, b_v, m_s, m_j, and t are indices for conduction and valence bands, spin, magnetic quantum number, and an atom in the unit cell. Here, summation over t includes those atoms in the unit cell which have the core state of the specified energy ϵ_a. Using the conventional linear muffin-tin orbital (LMTO) notation[10] the matrix element has the form[11]

$$M^{b,\vec{k}}_{t,m_j,m_s} = \sum_{l,m} i^l (A^{b,\vec{k}}_{t,l,m} M^r_{t,l} + B^{b,\vec{k}}_{t,l,m} \dot{M}^r_{t,l}) M^a_{m_j,l,m,m_s}, \quad (2)$$

where l and m are angular momentum and magnetic quantum numbers of the valence and conduction states. $M^r_{t,l}$, $\dot{M}^r_{t,l}$, and $M^a_{m_j,l,m,m_s}$ are radial matrix element, its energy derivative, and angular matrix element, respectively, having the following properties:

$$M^{\mathrm{r}}_{t,l} = \int R_t(r)\, r\, \phi_{t,l}(r)\, r^2 dr, \quad (3)$$

$$\dot{M}^{\mathrm{r}}_{t,l} = \int R_t(r)\, r\, \dot{\phi}_{t,l}(r)\, r^2 dr, \quad (4)$$

$$M^{\mathrm{a}}_{m_j,l,m,m_s} = \langle j, m_j | \hat{\epsilon} \cdot \hat{r} | l, m, m_s \rangle, \quad (5)$$

where $R_t(r)$ is the radial part of the core-level wave function and $\phi_{t,l}(r)$ is that of the valence or conduction band, $\hat{\epsilon}$ is the polarization vector of the photon, j refers to the total angular momentum of the core state, and $\langle j, m_j|$ and $|l, m, m_s\rangle$ are the angular parts of the core and valence/conduction states, respectively. The matrix element leads to the selection rules between the initial and final electronic states in the

absorption and emission of a photon in the scattering process ($\Delta l = \pm 1$). The localized core electron state of an atom t centered at a point $\vec{r}_a$ is

$$\phi^a_{t,m_j}(\vec{r}) = R_t(|\vec{r} - \vec{r}_a|)|j, m_j\rangle. \quad (6)$$

$A^{b\vec{k}}_{t,l,m}$ and $B^{b\vec{k}}_{t,l,m}$ are coefficients which depend on the crystal structure and the potential of the investigated system. The wave function of the valence and conduction electrons has the form

$$\Psi^{b\vec{k}}(\vec{r}) = \sum_{t,l,m} i^l [A^{b\vec{k}}_{t,l,m}\phi_{tl}(r) + B^{b\vec{k}}_{t,l,m}\dot{\phi}_{tl}(r)]|l, m, m_s\rangle, \quad (7)$$

where $\phi_{tl}(r)$ and $\dot{\phi}_{tl}(r)$ are the partial wave and its energy derivative, respectively. LMTO wave functions are linearized with respect to energy at some suitable fixed energy $E_{\nu l}$. Because we are interested in energy eigenvalues $E_{b\vec{k}}$ near $E_{\nu l}$, in the matrix elements (2) we can substitute $B^{b\vec{k}}_{t,l,m}$ coefficients by their approximate form $A^{b\vec{k}}_{t,l,m}(E_{b\vec{k}} - E_{\nu l})$, which reduces the required memory in computations by about a factor of two.

The electronic structure calculations were performed using the scalar-relativistic tight-binding linear muffin-tin orbital method in the atomic sphere approximation.[12] The valence states consisted of Mg $3s$, $3p$, and $3d$ states and B $2s$, $2p$, and $3d$ states. The hexagonal unit cell contained three atoms and three empty spheres. We used lattice parameters $a = b = 2.99$ Å and $c = 3.41$ Å corresponding to equilibrium volume in our calculations. For the exchange-correlation potential, the parametrized form by Perdew and Zunger[13] was used. The number of $\vec{k}$ points was 648 in the whole Brillouin zone.

The geometry used in the calculations is the following. The direction of the absorbed photon makes an angle of θ with respect to the hexagonal c axis of the MgB_2 single crystal. The absorbed photon is linearly polarized and the polarization is in the plane containing the direction of the photon and the c axis of the crystal. In this way the component of the polarization vector of the absorbed photon along the c axis can be varied from 0 to 1 by increasing θ from 0° to 90°. The direction of the emitted photon is perpendicular to the direction of the absorbed photon and makes a 90° $-\theta$ angle with respect to the c axis. For the emitted photon we have used two different linear polarizations. The polarization is either in the (a,b) plane or along the direction of the absorbed photon. All our results are expressed using an energy scale where the Fermi energy is 0 eV.

Overall features of both XES and XAS of MgB_2 are well produced by band-structure calculations.[14] Thus, RIXS experiments are also expected to be explained within the ordinary band-structure picture. Because the valence hole is delocalized and the $1s$ core hole in boron is well screened,[15] it is reasonable to use ground-state orbitals to obtain theoretical spectra. Due to the conservation of both energy and momentum, we need detailed band-structure data in order to interpret the spectra. The calculated band structure is shown in

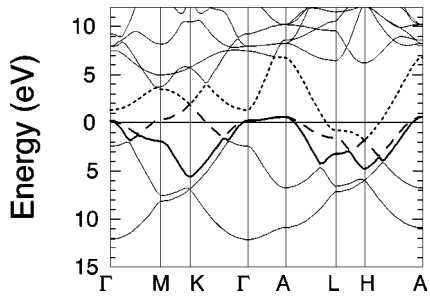

FIG. 1. Band-structure of MgB_2. Bands 3, 4, and 5, which cross the Fermi level, are shown by a thicker line: solid, dashed, and dotted, respectively.

Fig. 1. Since we are interested in absorption and emission of photons coupled with electron states near the Fermi energy, the most relevant bands are those which cross the Fermi level, i.e., band numbers 3–5. Zhang *et al.*[16] have measured RIXS spectra at different angles of incidence ($\theta = 15°, 45°$, and 60° with respect to the c axis of the MgB_2 crystal) and using different excitation energies (187.25 eV–188.25 eV, Fermi energy: $E_F = 187.28$ eV). They found two peaks in their spectra. The intensity of the peak just below the Fermi energy depends clearly on both direction and energy of the exciting radiation. On the other hand, the intensity of the peak at about 2 eV below the Fermi energy was considered to be unchanging.

In Fig. 2 we show our results for the $\theta = 60°$ incidence in the case of two polarizations of the emitted photon. The unpolarized emission spectrum is an average of these two extreme cases. The strong peak just below the Fermi energy is solely due to absorption to band 4 and emission from band 3. The features between -4 eV and -1.5 eV consist almost entirely of RIXS, involving band pairs (3,5) and (4,5). The calculated broad structure ranging from -8 eV to -5 eV appears as a tail in the measured spectra. These energy positions of the main structures of the calculated spectrum correspond well with the experimental values.[16]

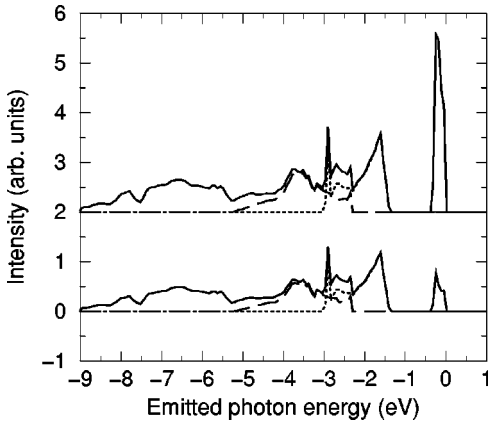

FIG. 2. Resonant inelastic x-ray scattering spectra calculated at $\theta = 60°$. Excitation energy is 0.2 eV relative to the Fermi energy. Polarization of the emitted photon is in the (a,b) plane (upper spectrum) and in the direction of the absorbed photon (lower spectrum). Dashed and dotted lines correspond to spectra calculated using bands (3,5) and (4,5), respectively.

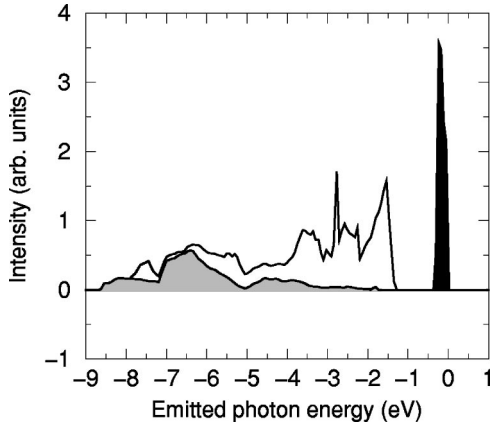

FIG. 3. Decomposition of the spectrum [$\theta = 60°$, excitation energy 0.2 eV, polarization of the emitted photon in the (a,b) plane]. The shaded parts show the resonant inelastic x-ray scattering related to absorption to the band 4, followed by emission from bands 1–3. The black and gray shadings correspond to the sections of band 4 around the Γ-A and M-K lines, respectively.

Figure 3 shows the absorption to band 4 and emission from bands 1–3 contained in the above spectrum [polarization of the emitted photon in the (a,b) plane]. Band number 4 includes two separate hole-like sheets of the Fermi surface: the cylindrical bonding $p_{x,y}$ band around the Γ-A line and the tubular bonding p_z band around the M-K line in the Brillouin zone.[17] To analyze the contributions related to these two regions of the Brillouin zone, we have split the calculation in the $\vec{k}$ space into two parts having $\vec{k}$ points either inside a Γ-A axial cylinder or outside it. As seen from Fig. 3, the cylindrical and tubular sheets of the Fermi surface contribute to the spectrum in clearly distinct energy regions, enabling the investigation of these sheets independently.

By increasing angle θ, one can measure more directly the excitations to the π band. In Fig. 4 we show the calculated

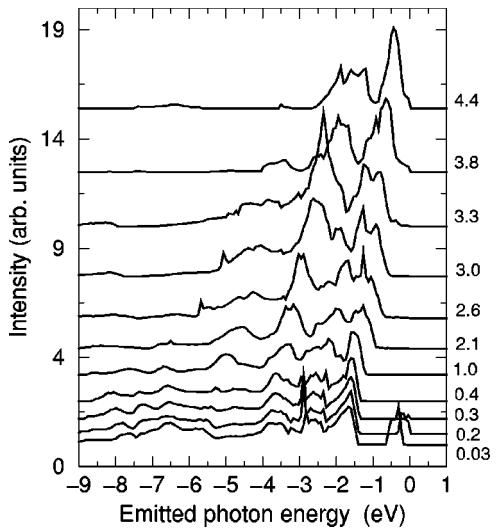

FIG. 4. Resonant inelastic x-ray scattering spectra calculated at $\theta = 75°$. Excitation energy (in eV), relative to the Fermi energy, is shown beside each spectrum. Polarization of the emitted photon is in the (a,b) plane.

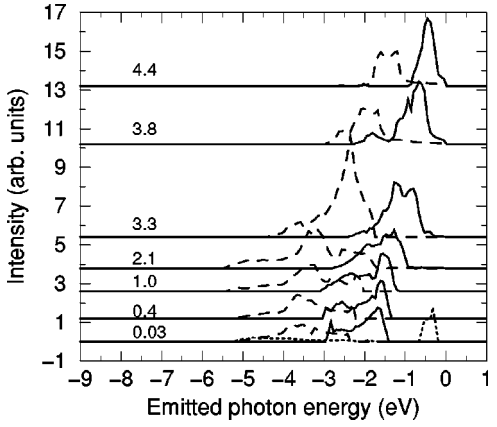

FIG. 5. Some of the spectra shown in Fig. 4 calculated using the bands (3,4) (dotted), (3,5) (dashed), and (4,5) (solid).

spectra corresponding to $\theta = 75°$ and the polarization of the emitted radiation in the ab plane. Near the top of the valence band there appears a peak which disappears when the excitation reaches 0.4 eV above the Fermi energy. The broad structure from -4 eV to -1.5 eV does not show much dispersion up to excitation energies 0.4 eV above the Fermi energy. However, using excitation energies above 1 eV, the intensity of the peaks increases considerably and the position of the peaks shifts about 1 eV closer to the Fermi level, as the excitation energy increases. To decide what bands and what parts of the Brillouin zone are responsible for each peak in the spectrum, we have calculated some of the spectra band by band. As Fig. 5 shows, the peak around -2 eV (low excitation energies) is mainly due to transitions involving bands 4 and 5. In the same way, the peak around -3.5 eV is mainly due to transitions involving bands 3 and 5. From Fig. 1 we see that both of these peaks are produced close to the L-H line in the Brillouin zone. In this region, near the Fermi energy, the constant energy surfaces of the antibonding π band have a tubular form.[17]

In summary, we have calculated RIXS spectra of MgB_2 using Kramers-Heisenberg formula with TB-LMTO eigenvalues and eigenstates for occupied and unoccupied electron states. The results presented indicate that MgB_2 can be analyzed and interpreted on the basis of ground-state band-structure calculations. The Fermi surface and phenomena related to that play an important role in the conductivity of materials. Our calculations show that the three physically different sheets of the Fermi surface of MgB_2 induce structures in RIXS spectra which are well separated in energy. This enables experimental investigation of each of them separately. In addition, we predict nonlinear emission structures related with the excitation of 1s electrons to the unoccupied antibonding π band in the neighborhood of the L-H line in the Brillouin zone.

We acknowledge computer resources of CSC–Scientific Computing Ltd., Espoo, Finland. This work has been supported in part by the Academy of Finland, Grant No. 51583 (K.K. and V.K.) and the Turku University Foundation (K.K. and W.H.).

*Author to whom correspondence should be addressed. Electronic address: kokko@utu.fi

[1] J. Akimitsu, Symposium on Transition Metal Oxides, Sendai, January 10, 2001.

[2] J. Nagamatsu, N. Nakagawa, T. Muranaka, Y. Zenitani, and J. Akimitsu, Nature (London) **410**, 63 (2001).

[3] R.P. Vasquez, C.U. Jung, Min-Seok Park, Heon-Jung Kim, J.Y. Kim, and Sung-Ik Lee, Phys. Rev. B **64**, 052510 (2001).

[4] H. Uchiyama, K.M. Shen, S. Lee, A. Damascelli, D.H. Lu, D.L. Feng, Z.-X. Shen, and S. Tajima, Phys. Rev. Lett. **88**, 157002 (2002).

[5] E.Z. Kurmaev, I.I. Lyakhovskaya, J. Kortus, A. Moewes, N. Miyata, M. Demeter, M. Neumann, M. Yanagihara, M. Watanabe, T. Muranaka, and J. Akimitsu, Phys. Rev. B **65**, 134509 (2002).

[6] A. Kotani and S. Shin, Rev. Mod. Phys. **73**, 203 (2001).

[7] J.A. Carlisle, E.L. Shirley, L.J. Terminello, J.J. Jia, T.A. Callcott, D.L. Ederer, R.C.C. Perera, and F.J. Himpsel, Phys. Rev. B **59**, 7433 (1999).

[8] Y. Ma, Phys. Rev. B **49**, 5799 (1994); P.D. Johnson and Y. Ma, *ibid.* **49**, 5024 (1994).

[9] W. Hergert, K. Kokko, and R. Laihia (unpublished).

[10] H.L. Skriver, *The LMTO Method*, edited by M. Cardona and P. Fulde, Springer Series in Solid-State Sciences Vol. 41 (Springer, Berlin, 1984).

[11] R. Laihia, K. Kokko, W. Hergert, and J.A. Leiro, Phys. Rev. B **58**, 1272 (1998).

[12] O.K. Andersen, O. Jepsen, and D. Glötzel, *Proc. Int. School of Physics 'Enrico Fermi' (Course LXXXIX) Highlights of Condensed-Matter Theory*, edited by F. Bassani, F. Fumi, and M.P. Tosi (North-Holland, Amsterdam, 1985), p. 59.

[13] J.P. Perdew and A. Zunger, Phys. Rev. B **23**, 5048 (1981).

[14] J. Nakamura, N. Yamada, K. Kuroki, T.A. Callcott, D.L. Ederer, J.D. Denlinger, and R.C.C. Perera, Phys. Rev. B **64**, 174504 (2001).

[15] K. Kokko, V. Kulmala, and J.A. Leiro, Phys. Rev. B **66**, 165114 (2002).

[16] G.P. Zhang, G.S. Chang, T.A. Callcott, D.L. Ederer, W.N. Kang, Eun-Mi Choi, Hyeong-Jin Kim, and Sung-Ik Lee, Phys. Rev. B **67**, 174519 (2003).

[17] J. Kortus, I.I. Mazin, K.D. Belashchenko, V.P. Antropov, and L.L. Boyer, Phys. Rev. Lett. **86**, 4656 (2001). See Fig. 3 in their article, where the antibonding p_z band gives the red tubular part of the Fermi surface around the L-H line.